BNL-211695-2019-JAAM

Room Temperature in vacuo Chemisorption of Xenon Atoms on Ru(0001) under Interface Confinement

J. Zhong, J. A. Boscoboinik

To be published in "The Journal of Physical Chemistry C"

April 2019

Center for Functional Nanomaterials

Brookhaven National Laboratory

U.S. Department of Energy

USDOE Office of Science (SC), Basic Energy Sciences (BES) (SC-22)

DISCLAIMER

Room Temperature *in vacuo* Chemisorption of Xenon Atoms on Ru(0001) under Interface Confinement

Jian-Qiang Zhong[†*], *Mengen Wang*[†,‡], *Nusnin Akter*[†,‡], *Dario J. Stacchiola*[†], *Deyu Lu*[†*], *J. Anibal Boscoboinik*[†*]

[†] Center for Functional Nanomaterials, Brookhaven National Laboratory, Upton, NY 11973, United States.

[‡] Materials Science and Chemical Engineering Department, Stony Brook University, Stony Brook, NY 11790, United States.

ABSTRACT Molecules confined at the nanoscale can exhibit intriguing physical and chemical properties. We report here the direct observation of room temperature *in vacuo* chemisorption of xenon (Xe) atoms on Ru(0001) under spatial confinement. Weakly bound two-dimensional (2D) silica bilayer films consisting of hexagonal prisms (~ 0.5 nm) were synthesized on a Ru(0001) substrate. The distance between the 2D-silica and the Ru(0001) surface can be controlled by changing the coverage of oxygen chemisorbed on Ru(0001), creating an interfacial space of tunable sub-nanometer thickness. Individual Xe atoms are trapped at 300 K in this nano-sized volume. Combined *in-situ* synchrotron-based X-ray photoelectron spectroscopy (XPS) and density functional theory (DFT) studies reveal that the hybridization between Xe and Ru orbitals

leads to the formation of a Xe-Ru bond with a significant amount of charge transfer, which can explain the observed core-level binding energy shifts in the XPS measurements. This work opens exciting opportunities to study the chemistry of individual noble gas atoms under extreme confinement.

INTRODUCTION

Xenon (Xe), like other noble gas atoms, is characterized by a relatively low chemical reactivity owing to its stable electronic configuration with full valence electron shells.[1] Xe used to be considered as inert until 1962 when Bartlett discovered that it can be oxidized by platinum hexafluoride (PtF_6) to form a mixture of various Xe-containing salts.[2,3] Many xenon compounds have been synthesized since then. For example, xenon halides can be synthesized by photochemical methods and discharge techniques[4,5], while xenon oxides/oxyhalides can be obtained through the hydrolysis of xenon fluorides in water[6,7]. The reactivity of Xe has been conjectured to be the main cause of the "missing xenon paradox", i.e., the anomalously low (by a factor of 20) Xe content in the Earth's atmosphere in comparison with other noble gases.[8] One hypothesis to reconcile this paradox suggests that Xe is stored either in minerals[8-10] or even deeper in the Earth under geological pressures as xenon oxides[11,12] or intermetallic compounds[13]. Over the past few decades, both experimental and theoretical efforts have been made to identify different types of chemical bonds in Xe compounds, such as ionic bonds, metallic bonds and covalent bonds[14-18]. Very recently, Frontera *et al*. reported a new noncovalent interaction between a covalently bonded Xe atom and a negative site (e.g., an anion or a Lewis base), namely aerogen bonding.[19]

Despite the intensive research on xenon compounds, the nature of the interaction between Xe and metal surfaces remains controversial.[20] The adsorption of Xe on metal surfaces was widely regarded as the paradigm of a physisorption process via noncovalent interactions (e.g., van der Waals interaction).[21] Bagus *et al*. concluded that the formation of Xe-metal interface dipole purely originates from "exchange-like" effects instead of from chemical effects or electrostatic interactions.[21] However, the physisorption picture has been challenged by a "covalent-like" interaction model based on computational studies.[22,23] Silva *et al*. observed characteristics of chemical interactions between Xe and metal surfaces, which were explained in terms of polarization and Pauli repulsion effects.[20] Several low-energy electron diffraction (LEED) studies at cryogenic temperatures have experimentally demonstrated an on-top site adsorption preference for Xe adatoms on closed-packed metal surfaces (e.g., Cu(111)[24], Pd(111)[25], Ru(0001)[26], and Pt(111)[27]). These on-top site preferences were attributed to their larger polarization and weaker Pauli repulsion, which were accompanied with broadened metal *d* orbitals, indicating the possibility of orbital hybridization with Xe adatoms.

Recently, two-dimensional (2D) (alumino)silicates of stoichiometry $Al_xSi_{1-x}O_2$, with $0 \leq x < 0.5$), were synthesized and proposed as 2D-zeolite models because of their similar chemical properties.[28] These structures consist of hexagonal prism nano-cages forming a 2D-array on a flat metallic surface. A pure SiO_2 version of this 2D-material had been previously reported by Loffler *et al*.[29] In addition to their applications in catalysis[30,31], we have previously demonstrated that these 2D-zeolite models can trap individual noble gas atoms in the nano-cages and, for the case of the pure SiO_2 structure, also at the 2D-silica/Ru(0001) interface.[32] These two types of nano-sized confinement offer exciting opportunities for surface science studies of chemistry in confined spaces, as described in a recent topical review.[33] In the present study, we explore the

chemistry of Xe atoms confined at the interface between the inert 2D-silica film and the Ru(0001) surface. The nature of the Xe-Ru interaction was investigated by *in-situ* synchrotron-based X-ray photoelectron spectroscopy (XPS) and further interpreted using density functional theory (DFT). Our results show covalent bonding between Xe and Ru, with significant orbital hybridization between Xe atoms and the Ru(0001) substrate.

EXPERIMENTAL AND COMPUTATIONAL METHODS

The Ru(0001) single crystal surface was cleaned with cycles of Ar^+ sputtering and annealing at 1400 K. It was then exposed to 3×10^{-6} mbar O_2 at 1200 K in order to form a chemisorbed *p*(2×2)-3O overlayer. The silica bilayers were grown on this *p*(2×2)-3O/Ru(0001) surface. Briefly, Si was thermally evaporated onto a *p*(2×2)-3O/Ru(0001) surface at room temperature under 2×10^{-7} mbar of O_2, followed by oxidation at 1200 K in 3×10^{-6} mbar O_2 for 10 minutes and slowly cooled down under the same O_2 pressure. Ambient pressure XPS (AP-XPS) measurements were carried out at the 23-ID-2 beamline (IOS) of the National Synchrotron Light Source II (NSLS-II).[34] The main chamber (base pressure 2×10^{-9} mbar) of the end-station was equipped with a differentially pumped hemispherical analyzer (Specs Phoibos 150 NAP), which was offset by 70° from the incident synchrotron light. Xe was introduced into the main chamber through a precision variable leak valve for the adsorption studies.

DFT calculations were performed using the projector augmented wave method implemented in the Vienna Ab initio simulation package (VASP)[35,36]. The consistent exchange van der Waals density functional (vdW-DF-cx)[37,38] was used to describe the non-local vdW interactions. Although Xe can be trapped both inside the nano-cage (Xe_{cage}) and at the silica/Ru(0001) interface (Xe_{int}), in the rest of this work we will mostly focus on the chemical properties of Xe_{int}

under nano confinement. The atomic structure of a Xe atom trapped at the silica/O/Ru(0001) interface is modeled by a 10.784 Å × 9.339 Å × 27 Å super cell with 4 silica nano-cages. Our model corresponds to a Xe coverage of $\Theta(Xe_{int}) = 0.25$, where $\Theta(Xe_{int})$ or $\Theta(Xe_{cage})$ is defined as the number of Xe atoms per 25.2 $Å^2$, the same size of the nano-cage. Five layers of Ru atoms were used to model the Ru(0001) substrate with chemisorbed O_{int} atoms. The Brillouin zone was sampled with 4×4×1 and a kinetic energy cutoff of 800 eV was used. The silica bilayer, Xe atoms, chemisorbed O atoms and top two layers of Ru atoms were allowed to relax in the structural optimization until forces were smaller than 0.01 eV/Å. Core-level binding energies (E_{BE}) were calculated using the transition state model of the excited systems.[39,40]

RESULTS AND DISCUSSIONS

Xe adsorption in the 2D-silica/Ru(0001) system is demonstrated *in-situ* by AP-XPS. The building unit of such bilayer framework is the hexagonal prism nano-cage (~ 0.5 nm) shown in Figure 1a – c. There are two nanoscale volumes that can host molecular species in this system, as denoted by an open and a filled star in Figure 1b: the hexagonal prim nanocages (open star) and the interface between the 2D-silica and the Ru(0001) surface (filled star). The 2D-silica/Ru(0001) interface distance strongly depends on the coverage of surface chemisorbed oxygen on Ru(0001) as described in the literature.[41,42]

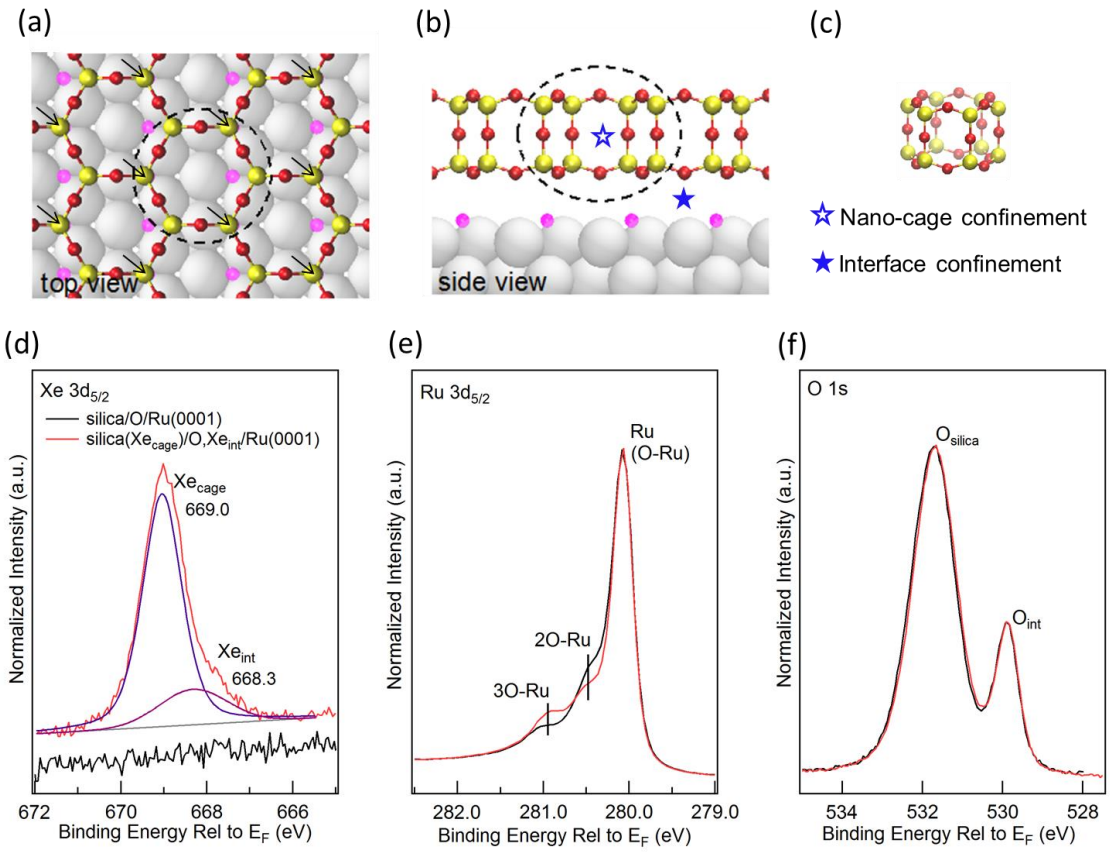

Figure 1. Structure of the 2D silica bilayer and surface confined Xe atoms in silica/Ru(0001). (a) Top and (b) side views of the 2D silica bilayer film adsorbed on *p*(2×1)-O/Ru(0001) surface (i.e., silica/O_{2x1}/Ru(0001)). (c) Illustration of the nano-cage in the framework and Xe sites under two types of confinements as indicated in (b), where the hollow star corresponds to the nano-cage while the solid star corresponds to the interface between the silica framework and the Ru(0001) surface. Color code: Ru (silver), Si (yellow), O in silica (red) and O chemisorbed on Ru surface (pink). Black arrows in (a) indicate the location of those chemisorbed oxygen atoms underneath silicon atoms. UHV XPS core level spectra of (d) Xe $3d_{5/2}$, (e) Ru $3d_{5/2}$, and (f) O 1s. The spectra before Xe exposure are in black and after Xe exposure are in red. The spectra intensity is normalized to the background on the lower binding energy side of the spectrum. Photon energy, $h\upsilon$ = 983 eV.

The silica/Ru(0001) surface is first exposed to 1.4 torr Xe gas. Simultaneously acquired AP-XPS spectra show strong gas phase features corresponding to the Xe $3d_{5/2}$ core level, as shown in Figure S1. However, the gas phase peak disappears after pumping out the Xe gas from the chamber, while a peak located at the lower binding energy side remains even after evacuating the Xe gas. This peak is assigned to the adsorbed Xe atoms in silica/Ru(0001). It should be noted that the X-ray beam plays an essential role in facilitating the capturing of the Xe atoms[10,32], as Xe cations produced by the X-rays during the AP-XPS measurements are the ones being trapped and then neutralized as they enter the cage or go through the silica film. The trapping mechanism of Xe and other noble gases is described in separate work[10].

Careful analysis of this adsorbed Xe peak shows that it has a main component at 669.0 eV and a broad shoulder at 668.3 eV as displayed in Figure 1d, which are assigned to Xe_{cage} and Xe_{int}, respectively. These peak assignments are inferred from the angle dependent XPS measurements (Figure S2) and supported by DFT calculations, where the Xe 3d binding energy of Xe_{cage} is calculated to be ~0.5 eV higher than that of the Xe_{int}[10]. From the peak areas in Figure 1d, the ratio between Xe_{int} and Xe_{cage} is estimated to be ~0.25. By comparing the peak areas of Xe 3d and Si 2p, the trapping coverage $\Theta(Xe_{int})$ is estimated to be 0.015 (Figure S3).

The adsorption of Xe does not significantly affect the bilayer framework as evident by the lack of any changes in the O 1s (Figure 1f) and Si 2p (Figure S4) core levels upon the inclusion of Xe_{cage}. However, Xe_{int} induces a strong redistribution of the chemisorbed oxygen at the silica/Ru interface (O_{int}). As shown in Figure 1e, the Ru $3d_{5/2}$ peak of silica/Ru(0001) is characterized by three main features (280.05 eV, 280.45 eV, and 280.95 eV), which are attributed to the bare Ru or Ru bonded with an O atom (Ru-O), Ru bonded with two O atoms (Ru-2O), and three O atoms

(Ru-3O) (Figure S5), respectively.[43,44] The total coverage of these O_{int} atoms is estimated to be 0.58 monolayer (ML) as calculated from the ratio between chemisorbed oxygen and silica framework oxygen (Table S1). Such high O coverage corresponds to Ru(0001) mainly covered by *p*(2×1)-O and *p*(2×2)-3O phases. Upon the trapping of Xe_{int}, the O_{int} on Ru(0001) are redistributed, resulting in a decrease in the Ru-2O peak and an increase in the Ru-3O peak (Figure 1e, red spectrum).

The trapping of Xe_{int} also affects the XPS valence band spectra shown in Figure 2. Since the silica bilayer structure remains intact and the total coverage of O_{int} is unchanged (0.58 ML) during the adsorption processes, the differences in valence band spectra before and after Xe adsorption are mainly related to the charge redistribution induced by the Xe_{int}-Ru interaction and the O_{int} redistribution.

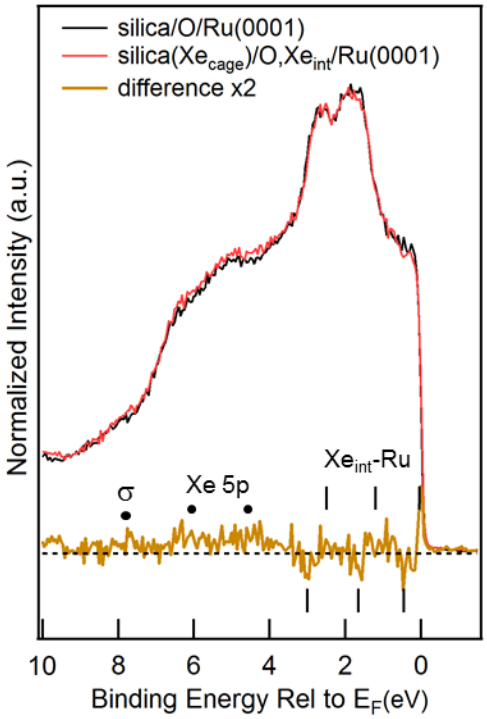

Figure 2. UHV XPS valence band spectra of silica/O/Ru(0001) and silica(Xe_{cage})/O,Xe_{int}/Ru(0001) (i.e., after 1.4 torr Xe exposure). The differences (the red curve minus the black curve) indicated in the figure are mainly related to the interactions between Xe_{int} and Ru. (Photon energy, $h\nu$ = 400 eV)

The interface confinement at the silica/Ru(0001) interface plays an important role in Xe_{int}-Ru interactions. As we previously reported, the coverage of chemisorbed O_{int} will strongly affect the properties at the silica/Ru(0001) interface.[42] For example, the interface distance between the silica and Ru(0001) (d_z(Ru-O_b)) can decrease by as much as 1.0 Å as O_{int} coverage decreases from 0.5 ML to 0 ML. Taking advantage of this relationship, we tuned the thickness of the confined interface for Xe_{int} by using H_2 to partially remove O_{int}.[34,45] Upon exposing the Xe/silica/Ru(0001) film to 1.2 torr H_2 gas at 300 K for 10 minutes, the total coverage of O_{int} decreases from 0.58 ML to 0.23 ML as calculated from the Ru $3d_{5/2}$ and O_{int} 1s peaks (the green spectra in Figure 3b and 3c). As a result, the magnitude of the surface dipole (O_{int}/Ru) caused by the charge transfer from Ru(0001) to O_{int} atoms decreases, and shifts all silica-related energy levels to higher binding energies (i.e., by 0.70 eV for O_{silica} 1s, 0.70 eV for Si 2p, and 0.65 eV for Xe_{cage} $3d_{5/2}$).

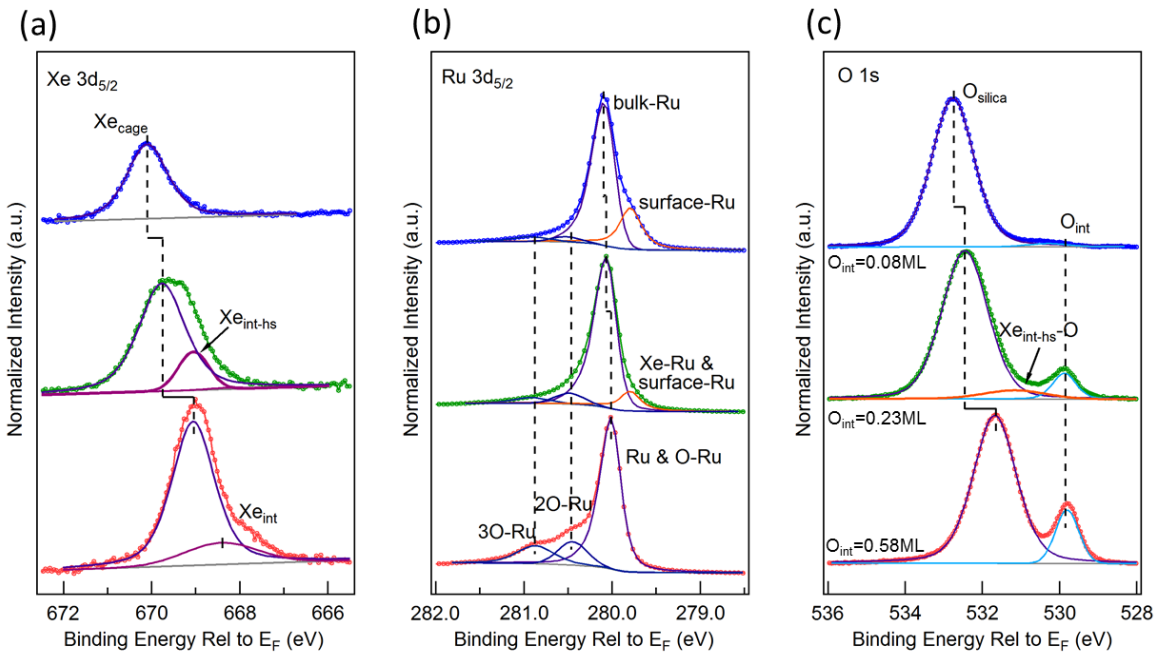

Figure 3. UHV XPS core level spectra of Xe adsorbed silica/O/Ru(0001). (a) Xe $3d_{5/2}$, (b) Ru $3d_{5/2}$, and (c) O 1s. The red spectra (bottom) are silica(Xe_{cage})/O,Xe_{int}/Ru(0001) after 1.4 torr Xe exposure with O_{int} coverage of 0.58 ML; the green spectra (middle) are silica(Xe_{cage})/O,$Xe_{int\text{-}hs}$/Ru(0001) after partially removing O_{int} (0.23 ML) by exposing the film to 1.2 torr H_2 gas at 300 K; the blue spectra (top) are silica(Xe_{cage})/Ru(0001) after almost completely removing O_{int} (0.08 ML) by further heating the film in 1.2 torr H_2 to 350 K. All spectra are taken in the UHV condition. (Photon energy, $h\upsilon$ = 983 eV)

Partial removal of the chemisorbed oxygen from the Ru(0001) surface from 0.58 ML to 0.23 ML creates an even more confined space at the interface. Based on DFT calculations, an O_{int} coverage change from 0.5 ML to 0.25 ML corresponds to a decrease of d_z(Ru-O_b) by 0.19 Å[42]. At a low coverage of Xe_{int} at $\Theta(Xe_{int})$= 0.015, we expect that changes in the silica-Ru(0001) distance due to the adsorption of Xe_{int} are negligible, because the small amount of Xe_{int} is not enough to push against the silica bilayer to offset the attractive force between the silica and

O/Ru(0001)[32]. Under a stronger silica-Ru(0001) attraction, Xe_{int} at the 0.23 ML oxygen coverage is subjected to an increased stress at the interface due to the reduction of the silica-Ru(0001) distance. Note that the "***stress***" here denotes the derivative of the total energy per unit area against the interface distance. We denote those Xe_{int} atoms subjected to the *higher stress* at the 0.23 ML oxygen coverage as $Xe_{int\text{-}hs}$, as compared to Xe_{int} at the 0.58 ML oxygen coverage.

The sharp peak at 669.05 eV in Figure 3a is therefore attributed to the $Xe_{int\text{-}hs}$. Due to this increased stress, $Xe_{int\text{-}hs}$ interacts more strongly with the Ru substrate and the bottom layer of the silica framework, as evidenced by a new feature of O 1s (Figure 3c) and the broadening of the Si 2p peaks (Figure S4). It should be noted that thermodynamically $Xe_{int\text{-}hs}$ is less stable than Xe_{int}, as the population of $Xe_{int\text{-}hs}$ determined from time-dependent XPS spectra decreases significantly after 50 minutes under the UHV conditions (Figure 4). The mechanism by which $Xe_{int\text{-}hs}$ desorbs is yet to be understood.

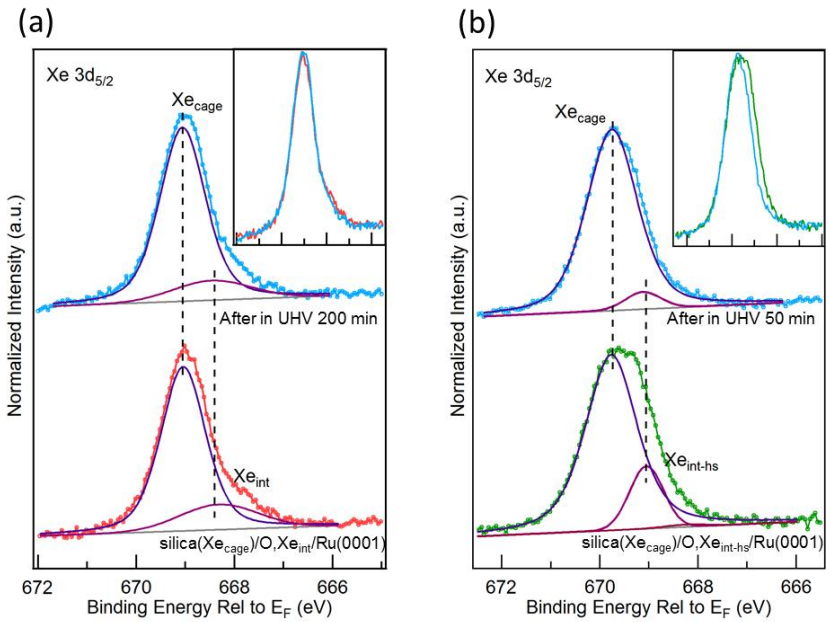

Figure 4. UHV XPS Xe $3d_{5/2}$ core level spectra of Xe adsorbed silica/O/Ru(0001). (a) The red spectrum is obtained after exposing silica/O/Ru(0001) to 1.4 torr Xe for 10 minutes [i.e., silica(Xe_{cage})/O,Xe_{int}/Ru(0001)] and the light-blue spectrum is obtained after sitting in the UHV chamber for 200 minutes. (b) The green spectrum is obtained after exposing silica(Xe_{cage})/O,Xe_{int}/Ru(0001) to 1.2 torr H_2 at 300K for 10 minutes [i.e., silica(Xe_{cage})/O,$Xe_{int\text{-}hs}$/Ru(0001)] and the light-blue spectrum is obtained after sitting in the UHV chamber for 50 minutes. (Photon energy, $h\nu$ = 983 eV).

By further heating the Xe-containing silica/Ru(0001) film in 1.2 torr H_2 to 350 K, O_{int} are almost completely removed, and all $Xe_{int\text{-}hs}$ desorb from the interface space. Some aspects of the kinetics of oxygen removal by hydrogen to produce water at this confined space were recently described by Prieto *et al.*[46]. As shown in the blue spectra in Figure 3a, $\Theta(Xe_{cage})$ decreases from 0.065 to 0.038 upon heating to 350 K in H_2. It should be noted that the Xe_{cage} is stable in UHV (up to 623 K) and in air at 300 K as we have recently demonstrated[10]. Upon removal of O_{int}, the core levels of Xe_{cage} $3d_{5/2}$ and O_{silica} 1s further shift to higher binding energies by ~ 0.40 eV due to the reduced surface dipoles.

Another interesting observation is that the O_{int} on Ru(0001) is spatially redistributed upon adsorption of interfacial Xe. The decrease in the 2O-Ru peak and the increase in the 3O-Ru peak (Figure 1e, red spectrum) suggest that likely O_{int} are redistributed unevenly with local clustering. In order to determine the favorable local oxygen environment surrounding the Xe_{int}, DFT calculations were performed to compare the total energies of Xe_{int} with different O_{int}/Ru surface models. Three configurations with a 0.5 ML O_{int} coverage and $\Theta(Xe_{int})$ = 0.25 are modeled. As shown in Figure 5a, there are equal amount of 2O-Ru and 1O-Ru under a uniform O_{int}

distribution (silica/(O_{2x1},Xe_{int})/Ru). In order to model a non-uniform O_{int} distribution, the Ru-2O is decreased to 25% and Ru-3O is increased to 18.75% with the rest 56.25% being either Ru-1O or clean Ru surface atoms as shown in Figure 6. Separate models are developed for Xe_{int} adsorbed in the O depleted area (Figure 6a) and O rich area (Figure 6b), respectively. It turns out that the former configuration is more stable than the latter by 0.85 eV, indicating that Xe_{int} atoms prefer to adsorb on the oxygen deficient region and, therefore, compete with O_{int} for Ru surface adsorption sites, which partially transforms the *p*(2×1)-O phase into the more dense *p*(2×2)-3O or *p*(1×1) phase.

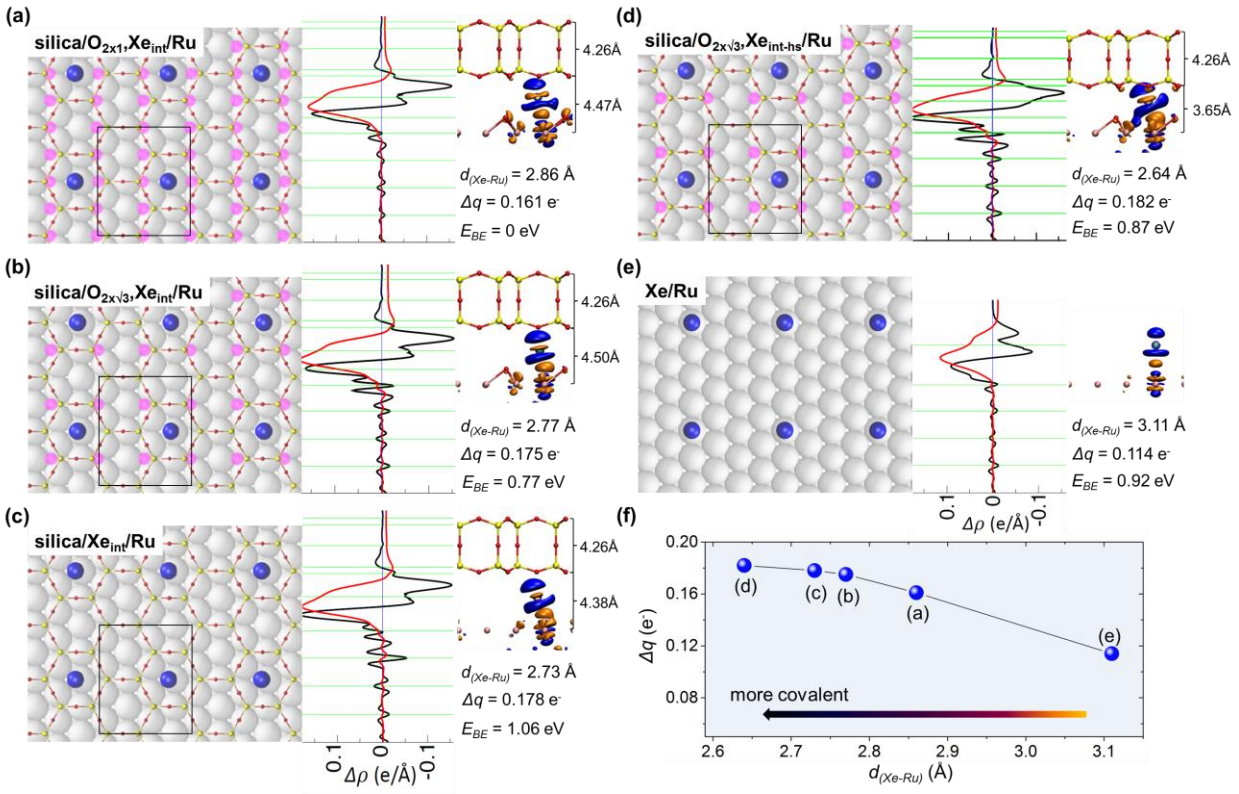

Figure 5. Relaxed structures of Xe_{int} ($\Theta(Xe_{int})$ = 0.25) adsorbed at the silica/Ru(0001) interface with (a) 0.5 ML O_{int} (silica/($O_{2\times1}$,Xe_{int})/Ru(0001)), (b) 0.25 ML O_{int} (silica/($O_{2\times\sqrt{3}}$,Xe_{int})/Ru(0001)) and (c) 0 ML O_{int} (silica/Xe_{int}/Ru(0001)). (d) Xe_{int} ($\Theta(Xe_{int})$ =

0.25) adsorbed at the silica/Ru(0001) interface with 0.25 ML O_{int} (silica/($O_{2\times\sqrt{3}}$,$Xe_{int\text{-}hs}$)/Ru(0001)) at a fixed interface distance of 3.65 Å. (e) Xe adsorbed on clean Ru(0001) (Xe/Ru(0001)). The black rectangles in left panels indicate the unit cell for each case; the middle panels show the integrated charge density difference (the black curves represent the integrated charge density difference as a function of *z*, and the red curves is the cumulative plot of black curves); the right panels show the isosurface of the charge density difference (orange: electron accumulation, blue: electron depletion and isovalue: 0.01 e/Å^3). E_{BE} is the calculated Xe_{int} core level binding energy relative to the Xe_{int} in silica/(O_{2x1},Xe_{int})/Ru(0001). Distances on the right correspond to the thickness of the silica film, $d_z(O_t\text{-}O_b)$, and the interface distance, $d_z(Ru\text{-}O_b)$. (f) Charge transferred from each Xe atom to the Ru substrate (Δq) as a function of $d_{Xe\text{-}Ru}$.

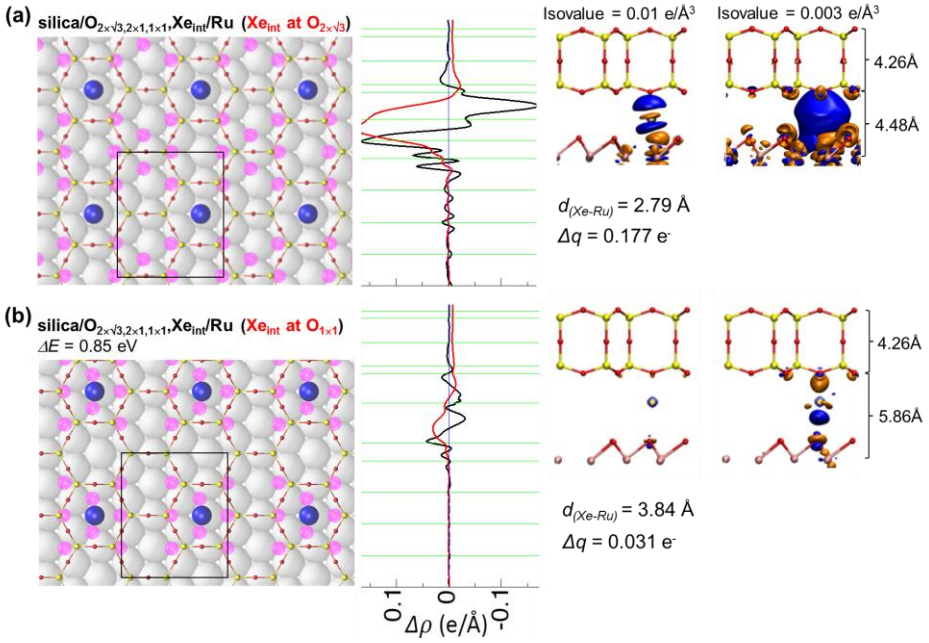

Figure 6. DFT calculated chemical interactions between the Xe_{int} and silica/Ru(0001). Adsorption of Xe_{int} will induce a redistribution of the O_{int}, i.e., from a $p(2\times1)$-O structure to mixed $p(2\times\sqrt{3})$-O, $p(2\times1)$-O and $p(1\times1)$-O structures. Total coverages of O_{int} are 0.5 ML for both

(a) and (b). Xe_{int} (Θ = 0.25) are simulated to adsorbed at either (a) $p(2\times\sqrt{3})$-O domain or (b) $p(1\times1)$-O domain, respectively. The left panels in Figure 6 (a) – (b) show the adsorption geometries and the black squares indicate the unit cell for each case. ΔE is the relative total energy of (b) compared with (a). The middle panels in Figure 6 (a) – (b) show the integrated charge density difference. The black curves represent the integrated charge density difference and the red curves represent the integration of the black curve. The right panels in Figure 6 (a) – (b) show the 3D plot of the charge density difference. The orange and blue regions correspond to electron accumulation and depletion, respectively. The isovalue is 0.01 e/Å^3 (left) and 0.003 e/Å^3 (right). $d_{(Xe\text{-}Ru)}$ is the distance between Xe and the bonded Ru atom. Δq represents the transferred electrons from Xe atoms to the Ru substrate. Distances on the right correspond to the thickness of the silica film ($d_z(O_t\text{-}O_b)$) and the interface distance ($d_z(Ru\text{-}O_b)$).

The charge transfer upon Xe_{int} adsorption is quantified by the charge density difference along the surface normal z direction defined as $\Delta\rho = \rho_{silica/Xe/Ru} - (\rho_{Xe} + \rho_{silica/Ru})$ integrated over the x-y plane, where the charge density is calculated for the combined system (silica/($O_{2\times1}$,Xe_{int})/Ru) and subsystems (Xe_{int} and silica/$O_{2\times1}$/Ru) at the optimized structures of silica/($O_{2\times1}$,Xe_{int})/Ru. The amount of the charge transfer (Δq) is calculated by integrating $\Delta\rho(z)$ in the z direction. As shown in Figure 5a, there is a net charge transfer (Δq) of 0.161 e^- from each Xe_{int} atom to the Ru substrate. The equilibrium Xe_{int}-Ru distance ($d_{Xe\text{-}Ru}$) is 2.86 Å after the structure optimization, which is similar to the sum of the covalent radii of Xe (1.40 Å) and Ru (1.46 Å), suggesting a covalent-like bond interaction.[47] There is a polarization in the O_{silica} atoms of the silica bilayer upon Xe_{int} adsorption as the charge density difference plot shown in Figure 6

with an isovalue of 0.003 e/Å^3, which could explain the new O 1s feature in Figure 3c. However, this effect is relatively small as compared with the Xe_{int}-Ru interaction.

After gradually removing chemisorbed surface oxygen to reach a coverage of 0.25 ML (silica/($O_{2\times\sqrt{3}}$,Xe_{int})/Ru(0001) in Figure 5b) and 0 ML (silica/Xe_{int}/Ru(0001) in Figure 5c), $d_{Xe\text{-}Ru}$ in our DFT calculations decreases to 2.77 Å and 2.73 Å, accompanied by Δq of 0.175 e^- and 0.178 e^- from Xe_{int} to Ru, respectively, suggesting stronger Xe_{int}-Ru interaction due to the enhanced interface confinements. The calculated core-level binding energies (E_{BE}) of Xe_{int} atom in silica/($O_{2\times\sqrt{3}}$,Xe_{int})/Ru(0001) is 0.77 eV higher than that of the Xe_{int} in silica/(O_{2x1},Xe_{int})/Ru(0001). The 0.77 eV shift results from the reduction of the Ru surface at lower surface oxygen coverage that reduces the negative surface dipole moment and the increase of Δq at the more confined interface. In order to separate the contributions from the surface dipole and Δq, half of the O_{int} in silica/(O_{2x1},Xe_{int})/Ru(0001) are removed with d_z(Ru-O_b) fixed at 4.47 Å, which is denoted as silica/(O'$_{2\times\sqrt{3}}$,Xe_{int})/Ru(0001). The calculated ΔE_{BE} for Xe_{int} in silica/(O'$_{2\times\sqrt{3}}$,Xe_{int})/Ru(0001) is 0.65 eV, which results from the reduced surface dipole. The remaining 0.12 eV in ΔE_{BE} is due to the increase of Δq at the more confined interface.

The relaxed interface distance d_z(Ru-O_b) in silica/($O_{2\times\sqrt{3}}$,Xe_{int})/Ru(0001) is 4.50 Å at $\Theta(Xe_{int})$ = 0.25 (Figure 5b). However, $\Theta(Xe_{int})$= 0.015 in the experiment is much lower that $\Theta(Xe_{int})$ = 0.25 used in our model. At such a low concentration, the small amount of Xe_{int} should have a negligible effect on d_z(Ru-O_b), and is highly unlikely to cause it to increase from 3.65 Å to 4.50 Å. However, modeling $\Theta(Xe_{int})$=0.015 requires a unit cell 17 times bigger than that at $\Theta(Xe_{int})$= 0.25, which becomes computationally intractable. Therefore, as shown Figure 5d, the case of $Xe_{int\text{-}hs}$ is approximated by silica/($O_{2\times\sqrt{3}}$,$Xe_{int\text{-}hs}$)/Ru(0001) with $\Theta(Xe_{int})$ = 0.25 but a fixed d_z(Ru-

O_b) at 3.65 Å, the same as the value in the silica/O/Ru system with O_{int} of 0.25 ML.[42] This extreme interface confinement further pushes Xe_{int} closer to the Ru substrate, resulting in a shorter $d_{Xe\text{-}Ru}$ of 2.64 Å and an increase of Δq to 0.182 e^-. Consequently, E_{BE} increases to 0.87 eV, which is consistent with the experimental data in Figure 3a, where the $Xe_{int\text{-}hs}$ $3d_{5/2}$ peak (middle) is shifted to higher binding energies by 0.75 eV when compared to the Xe_{int} peak (bottom).

These results indicate that Xe_{int}-Ru bond can be more covalent at the compressed silica-Ru(0001) interface. On a bare Ru(0001) surface, the equilibrium distance between the Xe and Ru atoms is 3.11 Å, as shown in Figure 5e. In the presence of the 2D-silica bilayer, the 2D-framework exerts a normal stress on the Xe atom. On one hand, this normal stress reduces the Xe-Ru distance to 2.73 Å (see Figure 5c), which leads to a stronger Xe-Ru hybridization with more covalent character. On the other hand, adsorption energies of Xe atoms at the silica/Ru interface become positive. The adsorption energy for Xe at the silica/4O/Ru interface is 0.77 eV, which is calculated by $\Delta E = E_{sub+Xe(trap)} - (E_{sub} + E_{Xe})$, where $E_{sub+Xe(trap)}$, E_{sub} and E_{Xe} are the total energies for silica/O/Ru(0001) with and without trapped Xe, and the isolated Xe atom, respectively. This positive Xe adsorption energy can be understood as the 2D-silica bilayer pushes Xe toward the Ru substrate by 0.38 Å, creating an energy penalty. Detailed analysis on the adsorption energy in a similar situation can be found elsewhere (Ref 10 and 32).

The degree of the Xe-Ru covalent interaction under different degrees of interface confinement is quantified by the amount of charge transfer as a function of $d_{Xe\text{-}Ru}$ in Figure 5f. Since a weak covalent-like interaction has been proposed for the adsorption of Xe on several transition metal surfaces at cryogenic temperatures,[20,26] Xe adsorbed on bare Ru(0001) surface without silica bilayer (Figure 5e) is shown for comparison. It is found that Xe sits on top of the Ru atoms with

a $d_{Xe\text{-}Ru}$ of 3.11 Å, accompanied with an charge transfer of 0.114 e^- (or an induced dipole moment of μ=0.30 eÅ). Xe interacts stronger with Ru(0001) than Pt(111) or Pd(111) from previous calculations using the Perdew-Burke-Ernzerhof functional, where $d_{Xe\text{-}Pt}$ is 3.62 Å with $\mu_{Xe\text{-}Pt}$ = 0.07 eÅ and $d_{Xe\text{-}Pd}$ is 3.41 Å with $\mu_{Xe\text{-}Pd}$ = 0.09 eÅ. These on-top adsorption preferences arise from the polarization and Pauli repulsion effects in addition to the van der Waals interaction.[20,22]. Confining the Xe atoms with a silica bilayer on the Ru(0001) significantly enhances the charge transfer and results in a Xe-Ru bond that is more covalent in nature (Figure 5f). It should be noted that the chemisorption-like behavior of Xe_{int} described here for the silica/Ru system takes place at room temperature, as opposed to Xe on the bare metal which requires cryogenic temperatures.[26]

To gain more insights into the Xe_{int}-Ru bond induced by interface confinement, we calculate the projected density of states (PDOS) of silica/Xe_{int}/Ru(0001) before and after Xe_{int} chemisorption. As indicated by the arrow in Figure 7a, there is an increase in the unoccupied Xe p_z states upon adsorption of Xe_{int}, indicating an electron depletion of the Xe_{int} atom. In comparison, such states are not present at silica/$O_{2\times\sqrt{3},2\times1,1\times1}$,$Xe_{int}$/Ru(0001), where Xe is adsorbed at the p(1×1)-O domain (Figure S7). The Xe p_z orbital hybridizes with Ru s and d_{z^2} orbital at -7 eV (1 eV) below (above) the Fermi level (E_F) to form a bonding state σ (an anti-bonding state σ^*) (Figure 7b). The electron accumulation in Ru is in d_{xz} and d_{yz} orbitals, mostly at energies deeper in the valence band (Figure 7c). The electron redistributions are consistent with the charge density difference plot in Figure 5. The stronger orbital hybridizations lower the Xe p_z peak as compared to the p_z peak of Xe in Xe/Ru(0001) (Figure S6) or silica/($O_{2\times\sqrt{3},1\times1}$,$Xe_{int}$)/Ru(0001) with Xe_{int} adsorbed at p(1x1)-O domain (Figure S7). Such behavior indicates a covalent bond formed between Xe_{int} and Ru atoms in silica/Xe_{int}/Ru(0001).

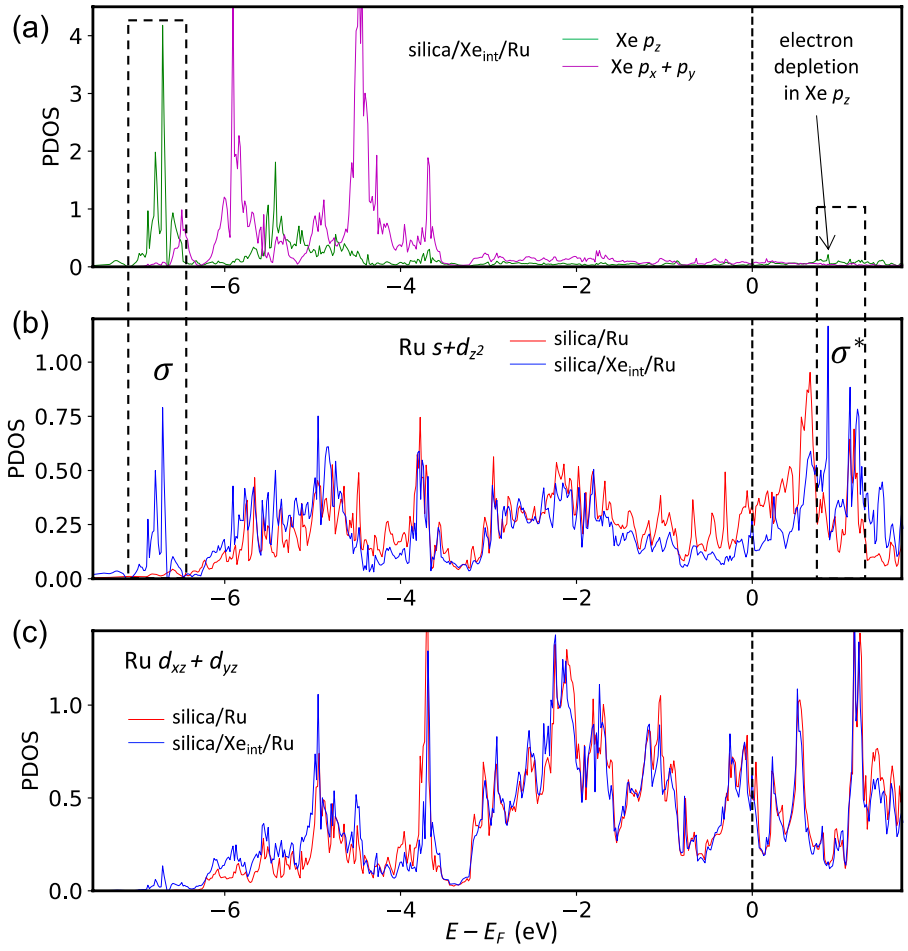

Figure 7. Projected density of states (PDOS) of silica/Xe$_{int}$/Ru(0001) and silica/Ru(0001). (a) PDOS of Xe p_z orbital and Xe p_x+p_y orbitals. (b) PDOS of Ru s and d_{z^2} orbitals. (c) PDOS of Ru $d_{xz} + d_{yz}$ orbitals. The energies are relative to E_F.

The chemistry of most xenon compounds usually contains electronegative atoms (e.g., fluorine and oxygen), to which Xe can donate electrons. For example, the thermodynamically stable Xe-O compounds can be formed under high pressures (~100 GPa).[11] The spatially confined Xe$_{int}$ atoms at the silica/Ru(0001) system can provide more insights into the less common case of covalent bonding between Xe and metallic surfaces. Moreover, our silica bilayer model has

shown the ability to mimic effective high stress conditions due to spatial confinement even inside a vacuum chamber and can act like a nano-container or nano-reactor.[48]

CONCLUSIONS

Individual Xe atoms can be immobilized at room temperature either in hexagonal prims nano-cages of a silica bilayer framework or at the interface between the silica and a Ru(0001) support. While Xe atoms in the nano-cages are physically trapped, the Xe atoms at the confined interface region show a significant covalent interaction with the Ru(0001) surface. Moreover, the strength of this Xe-Ru chemical interaction can be controlled by the interface distance. The intriguing chemistry of chemisorbed Xe evident upon increasing the effective force it is subjected to in the reduced space between the silica framework and the Ru(0001) surface provides a playground for exploring new xenon chemistry (and potentially for other species and reactions) induced by confinement effects.

ASSOCIATED CONTENT

Supporting Information

The Supporting Information is available free of charge on the ACS Publications website

Additional XPS spectra of Xe on silica/O/Ru(0001), PDOS of Xe/Ru(0001) and silica/$O_{2\times\sqrt{3},2\times1,1\times1,}Xe_{int}$/Ru(0001)

Corresponding Author

J.Q.Z (zjq.txt@gmail.com), D.L (dlu@bnl.gov) or J.A.B (jboscoboinik@bnl.gov)

Author Contributions

J.Q.Z. and J.A.B. were the main experimenters. M.W. and D.L. carried out the DFT calculations. J.Q.Z. and M.W. wrote the manuscript. All authors participated in discussions, data analysis and manuscript preparation.

Notes

The authors declare no competing financial interests.

ACKNOWLEDGMENTS

Research is carried out in part at the Center for Functional Nanomaterials, the 23-ID-2 (IOS) beamline of the National Synchrotron Light Source II, and the Scientific Data and Computing Center, a component of the Computational Science Initiative at Brookhaven National Laboratory, which are supported by the U.S. Department of Energy, Office of Basic Energy Sciences, under Contract No. DE-SC0012704. This research used resources of the National Energy Research Scientific Computing Center, a DOE Office of Science User Facility supported by the Office of Science of the U.S. Department of Energy under Contract No. DE-AC02-05CH11231. J.Q. Zhong and M. Wang are supported by BNL LDRD Project No. 15-010.

REFERENCES

(1) Mackay, R.A.; Henderson, W. *Introduction to Modern Inorganic Chemistry, 6th edition*; CRC Press 2002.

(2) Bartlett, N. Xenon Hexafluoroplatinate(V) Xe+[PtF6]-. *Proc. Chem. Soc.* **1962**, *112*, 218.

(3) Graham, L.; Graudejus, O.; Jha, N. K.; Bartlett, N. Concerning the Nature of XePtF6. *Coord. Chem. Rev.* **2000**, *197*, 321-334.

(4) Weeks, J. L.; Chernick, C. L.; Matheson, M. S. Photochemical Preparation of Xenon Difluoride. *J. Am. Chem. Soc.* **1962**, *84*, 4612-4613.

(5) Proserpio, D. M.; Hoffmann, R.; Janda, K. C. The Xenon-chlorine Conundrum: van der Waals Complex or Linear Molecule? *J. Am. Chem. Soc.* **1991**, *113*, 7184-7189.

(6) Brock, D. S.; Schrobilgen, G. J. Synthesis of the Missing Oxide of Xenon, XeO2, and Its Implications for Earth's Missing Xenon. *J. Am. Chem. Soc.* **2011**, *133*, 6265-6269.

(7) Smith, D. F. Xenon Oxyfluoride. *Science* **1963**, *140*, 899-900.

(8) Sanloup, C.; Schmidt, B. C.; Perez, E. M. C.; Jambon, A.; Gregoryanz, E.; Mezouar, M. Retention of Xenon in Quartz and Earth's Missing Xenon. *Science* **2005**, *310*, 1174-1177.

(9) Seoung, D.; Lee, Y.; Cynn, H.; Park, C.; Choi, K.-Y.; Blom, D. A.; Evans, W. J.; Kao, C.-C.; Vogt, T.; Lee, Y. Irreversible Xenon Insertion into a Small-pore Zeolite at Moderate Pressures and Temperatures. *Nat. Chem.* **2014**, *6*, 835.

(10) Zhong, J. Q.; Wang, M.; Akter, N.; Kestell, J. D.; Niu, T.; Boscoboinik, A. M.; Kim, T.; Stacchiola, D. J.; Wu, Q.; Lu, D. Ionization-Facilitated Formation of 2D (Alumino) Silicate-Noble Gas Clathrate Compounds. *Adv. Funct. Mater.* **2019**, 1806583.

(11) Zhu, Q.; Jung, D. Y.; Oganov, A. R.; Glass, C. W.; Gatti, C.; Lyakhov, A. O. Stability of Xenon Oxides at High Pressures. *Nat. Chem.* **2012**, *5*, 61.

(12) Dewaele, A.; Worth, N.; Pickard, C. J.; Needs, R. J.; Pascarelli, S.; Mathon, O.; Mezouar, M.; Irifune, T. Synthesis and Stability of Xenon Oxides Xe2O5 and Xe3O2 under Pressure. *Nat. Chem.* **2016**, *8*, 784.

(13) Zhu, L.; Liu, H.; Pickard, C. J.; Zou, G.; Ma, Y. Reactions of Xenon with Iron and Nickel are Predicted in the Earth's Inner Core. *Nat. Chem.* **2014**, *6*, 644.

(14) Grochala, W. Atypical Compounds of Gases, Which have been Called 'Noble'. *Chem. Soc. Rev.* **2007**, *36*, 1632-1655.

(15) Ehlers, A. W.; Frenking, G.; Baerends, E. J. Structure and Bonding of the Noble Gas−Metal Carbonyl Complexes M(CO)5−Ng (M = Cr, Mo, W and Ng = Ar, Kr, Xe). *Organometallics* **1997**, *16*, 4896-4902.

(16) Evans, C. J.; Lesarri, A.; Gerry, M. C. L. Noble Gas−Metal Chemical Bonds. Microwave Spectra, Geometries, and Nuclear Quadrupole Coupling Constants of Ar−AuCl and Kr−AuCl. *J. Am. Chem. Soc.* **2000**, *122*, 6100-6105.

(17) Kalinowski, J.; Räsänen, M.; Gerber, R. B. Chemically-Bound Xenon in Fibrous Silica. *Phys. Chem. Chem. Phys.* **2014**, *16*, 11658-11661.

(18) Seidel, S.; Seppelt, K. Xenon as a Complex Ligand: The Tetra Xenono Gold(II) Cation in $AuXe_4^{2+}(Sb_2F_{11}^-)_2$. *Science* **2000**, *290*, 117-118.

(19) Bauzá, A.; Frontera, A. Aerogen Bonding Interaction: A New Supramolecular Force? *Angew. Chem. Int. Ed.* **2015**, *54*, 7340-7343.

(20) Da Silva, J. L. F.; Stampfl, C.; Scheffler, M. Xe Adsorption on Metal Surfaces: First-principles Investigations. *Phys. Rev. B* **2005**, *72*, 075424.

(21) Bagus, P. S.; Staemmler, V.; Wöll, C. Exchangelike Effects for Closed-Shell Adsorbates: Interface Dipole and Work Function. *Phys. Rev. Lett.* **2002**, *89*, 096104.

(22) Müller, J. E. Interaction of the Pt(111) Surface with Adsorbed Xe Atoms. *Phys. Rev. Lett.* **1990**, *65*, 3021-3024.

(23) Clarke, S.; Bihlmayer, G.; Blügel, S. Chemical Effects in Rare Gas Adsorption: FLAPW Calculations for Ag(001)c(2x2)-Xe. *Phys. Rev. B* **2001**, *63*, 085416.

(24) Seyller, T.; Caragiu, M.; Diehl, R. D.; Kaukasoina, P.; Lindroos, M. Observation of Top-site Adsorption for Xe on Cu(111). *Chem. Phys. Lett.* **1998**, *291*, 567-572.

(25) Caragiu, M.; Seyller, T.; Diehl, R. D. Dynamical LEED Study of Pd(111)-(/3x/3)R30-Xe. *Phys. Rev. B* **2002**, *66*, 195411.

(26) Narloch, B.; Menzel, D. Structural Evidence for Chemical Contributions in the Bonding of the Heavy Rare Gases on a Close-packed Transition Metal Surface: Xe and Kr on Ru(001). *Chem. Phys. Lett.* **1997**, *270*, 163-168.

(27) Seyller, T.; Caragiu, M.; Diehl, R. D.; Kaukasoina, P.; Lindroos, M. Dynamical LEED Study of Pt(111)-(/3x/3)R30-Xe. *Phys. Rev. B* **1999**, *60*, 11084-11088.

(28) Boscoboinik, J. A.; Yu, X.; Yang, B.; Fischer, F. D.; Włodarczyk, R.; Sierka, M.; Shaikhutdinov, S.; Sauer, J.; Freund, H.-J. Modeling Zeolites with Metal-Supported Two-Dimensional Aluminosilicate Films. *Angew. Chem. Int. Ed.* **2012**, *51*, 6005-6008.

(29) Loffler, D.; Uhlrich, J. J.; Baron, M.; Yang, B.; Yu, X.; Lichtenstein, L.; Heinke, L.; Buchner, C.; Heyde, M.; Shaikhutdinov, S.; Freund, H. J.; Wlodarczyk, R.; Sierka, M.; Sauer, J. Growth and Structure of Crystalline Silica Sheet on Ru(0001). *Phys. Rev. Lett.* **2010**, *105*, 4.

(30) Boscoboinik, J. A.; Yu, X.; Shaikhutdinov, S.; Freund, H.-J. Preparation of an Ordered Ultra-thin Aluminosilicate Framework Composed of Hexagonal Prisms Forming a Percolated Network. *Micropor. Mesopor. Mater.* **2014**, *189*, 91-96.

(31) Boscoboinik, J. A.; Shaikhutdinov, S. Exploring Zeolite Chemistry with the Tools of Surface Science: Challenges, Opportunities, and Limitations. *Catal. Lett.* **2014**, *144*, 1987-1995.

(32) Zhong, J.-Q.; Wang, M.; Akter, N.; Kestell, J. D.; Boscoboinik, A. M.; Kim, T.; Stacchiola, D. J.; Lu, D.; Boscoboinik, J. A. Immobilization of Single Argon Atoms in Nano-cages of Two-dimensional Zeolite Model Systems. *Nat. Commun.* **2017**, *8*, 16118.

(33) Jorge Anibal, B. Chemistry in Confined Space through the Eyes of Surface Science - 2D Porous Materials. *J. Phys. Condens. Matter* **2018**, *31*, 063001

(34) Zhong, J.-Q.; Kestell, J.; Waluyo, I.; Wilkins, S.; Mazzoli, C.; Barbour, A.; Kaznatcheev, K.; Shete, M.; Tsapatsis, M.; Boscoboinik, J. A. Oxidation and Reduction under Cover: Chemistry at the Confined Space between Ultrathin Nanoporous Silicates and Ru(0001). *J. Phys. Chem. C* **2016**, *120*, 8240-8245.

(35) Kresse, G.; Furthmüller, J. Efficient Iterative Schemes for ab Initio Total-energy Calculations using a Plane-wave Basis Set. *Phys. Rev. B* **1996**, *54*, 11169.

(36) Kresse, G.; Furthmüller, J. Efficiency of ab-initio Total Energy Calculations for Metals and Semiconductors using a Plane-wave Basis Set. *Comput. Mater. Sci.* **1996**, *6*, 15-50.

(37) Bjorkman, T. Testing Several Recent van der Waals Density Functionals for Layered Structures. *J. Chem. Phys.* **2014**, *141*, 074708.

(38) Berland, K.; Hyldgaard, P. Exchange Functional that Tests the Robustness of the Plasmon Description of the van der Waals Density Functional. *Phys. Rev. B* **2014**, *89*, 035412.

(39) Wang, M.; Zhong, J.-Q.; Stacchiola, D. J.; Boscoboinik, J. A.; Lu, D. First-Principles Study of Interface Structures and Charge Rearrangement at the Aluminosilicate/Ru(0001) Heterojunction. *J. Phys. Chem. C* **2018**, *10.1021/acs.jpcc.8b05853*.

(40) Göransson, C.; Olovsson, W.; Abrikosov, I. A. Numerical Investigation of the Validity of the Slater-Janak Transition-state Model in Metallic Systems. *Phys. Rev. B* **2005**, *72*, 134203.

(41) Włodarczyk, R.; Sierka, M.; Sauer, J.; Löffler, D.; Uhlrich, J. J.; Yu, X.; Yang, B.; Groot, I. M. N.; Shaikhutdinov, S.; Freund, H. J. Tuning the Electronic Structure of Ultrathin Crystalline Silica Films on Ru(0001). *Phys. Rev. B* **2012**, *85*, 085403.

(42) Wang, M.; Zhong, J.-Q.; Kestell, J.; Waluyo, I.; Stacchiola, D. J.; Boscoboinik, J. A.; Lu, D. Energy Level Shifts at the Silica/Ru(0001) Heterojunction Driven by Surface and Interface Dipoles. *Top. Catal.* **2017**, *60*, 481-491.

(43) Lizzit, S.; Baraldi, A.; Groso, A.; Reuter, K.; Ganduglia-Pirovano, M. V.; Stampfl, C.; Scheffler, M.; Stichler, M.; Keller, C.; Wurth, W.; Menzel, D. Surface Core-level Shifts of Clean and Oxygen-covered Ru(0001). *Phys. Rev. B* **2001**, *63*, 205419.

(44) Over, H.; Seitsonen, A. P.; Lundgren, E.; Wiklund, M.; Andersen, J. N. Spectroscopic Characterization of Catalytically Active Surface Sites of a Metallic Oxide. *Chem. Phys. Lett.* **2001**, *342*, 467-472.

(45) Emmez, E.; Yang, B.; Shaikhutdinov, S.; Freund, H.-J. Permeation of a Single-layer SiO2 Membrane and Chemistry in Confined Space. *J. Phys. Chem. C* **2014**, *118*, 29034-29042.

(46) Prieto Mauricio, J.; Klemm Hagen, W.; Xiong, F.; Gottlob Daniel, M.; Menzel, D.; Schmidt, T.; Freund, H.-J. Water Formation under Silica Thin Films: Real-Time Observation of a Chemical Reaction in a Physically Confined Space. *Angew. Chem. Int. Ed.* **2018**, *57*, 8749-8753.

(47) Cordero, B.; Gomez, V.; Platero-Prats, A. E.; Reves, M.; Echeverria, J.; Cremades, E.; Barragan, F.; Alvarez, S. Covalent Radii Revisited. *Dalton Trans.* **2008**, 2832-2838.

(48) Fu, Q.; Bao, X. Surface Chemistry and Catalysis Confined under Two-dimensional Materials. *Chem. Soc. Rev.* **2017**, *46*, 1842-1874.

TOC Graphic

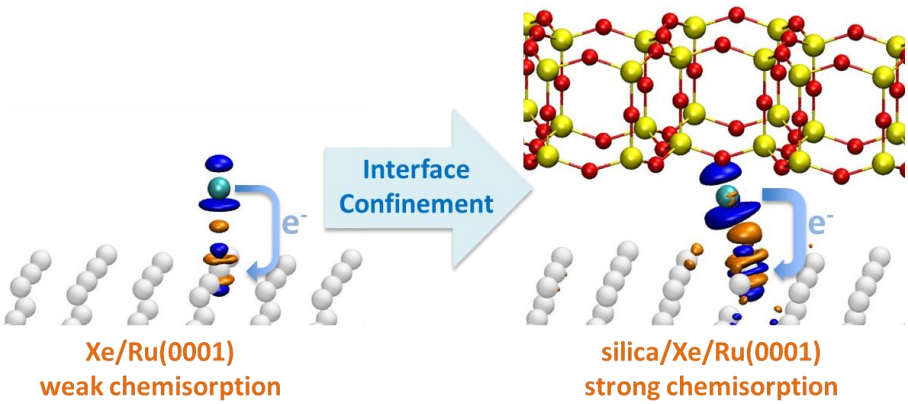
Interface
Confinement
e-
e-
Xe/Ru(0001)
weak chemisorption
silica/Xe/Ru(0001)
strong chemisorption

Supporting Information

Room Temperature *in vacuo* Chemisorption of Xenon Atoms on Ru(0001) under Interface Confinement

Jian-Qiang Zhong[†*], Mengen Wang[†,‡], Nusnin Akter[†,‡], Dario J. Stacchiola[†], Deyu Lu[†*], J. Anibal Boscoboinik[†*]

[†] Center for Functional Nanomaterials, Brookhaven National Laboratory, Upton, NY 11973, United States.

[‡] Materials Science and Engineering Department, Stony Brook University, Stony Brook, NY 11790, United States.

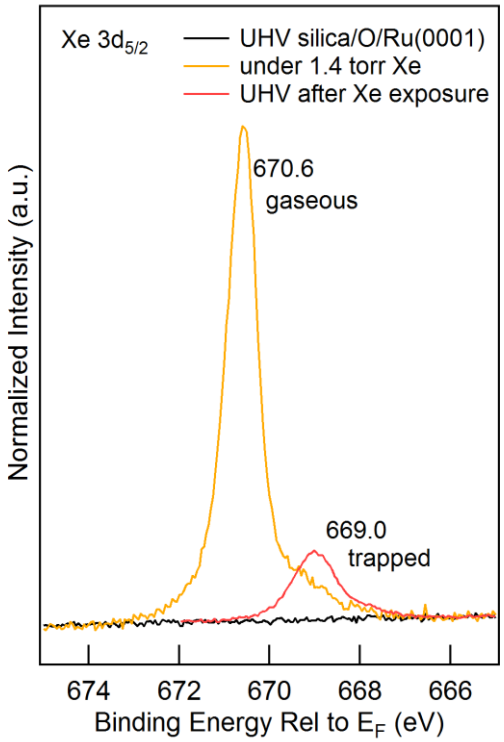

Figure S1. XPS core level spectra of Xe $3d_{5/2}$ on silica/O/Ru(0001). The black spectrum is obtained in UHV on clean silica bilayer, the yellow spectrum is obtained under 1.4 torr Xe gas environment, and the red spectrum is obtained in UHV after 1.4 torr Xe exposure for 10 minutes. (Photon energy, $h\upsilon$ = 983 eV)

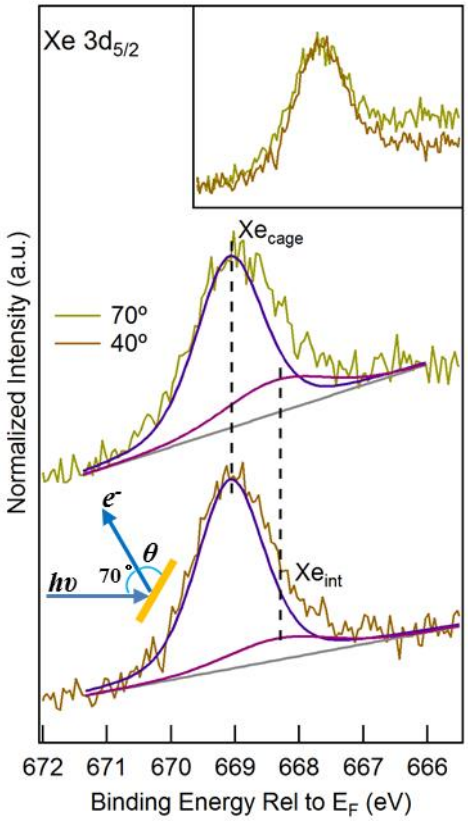

Figure S2. Angle dependent XPS core level spectra of Xe $3d_{5/2}$ on silica(Xe_{cage})/O,Xe_{int}/Ru(0001). Angle dependent XPS experiments were carried out to qualitatively determine the relative depth at which these Xe atoms are located. The shoulder at the lower binding energies becomes comparatively stronger at the larger θ = 70° photoelectron emission angle (θ, with respect to the surface plan) when compared to the spectra taken at θ = 40°. This indicates that the shoulder corresponds to Xe atoms at a deeper location and are assigned to the interface between the silica framework and the Ru(0001) surface (Xe_{int}), while the main peak is assigned to Xe atoms within the hexagonal nano-cages (Xe_{cage}). Spectra were obtained in UHV after 2 torr Xe exposure for 10 minutes. (Photon energy, $h\upsilon$ = 983 eV)

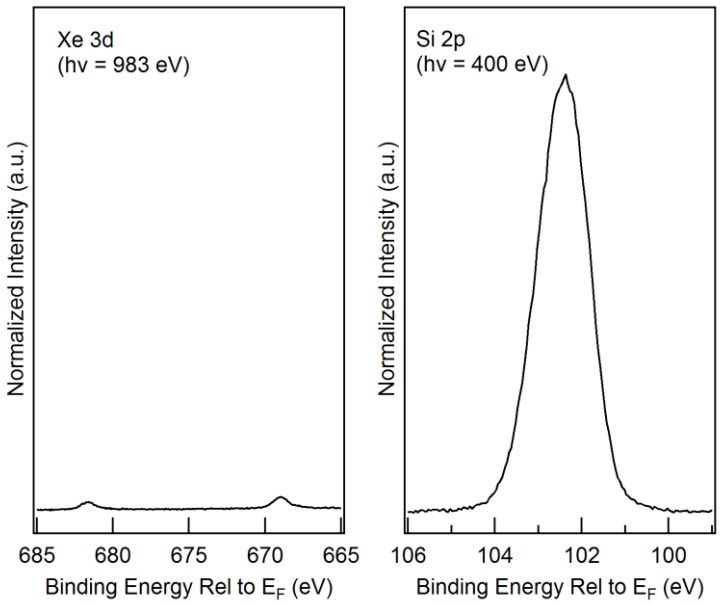

Figure S3. UHV XPS core level spectra of Xe 3d and Si 2p of the silica bilayer after 1.4 torr Xe gas exposure. Different photon energies are used in order to have similar photoelectron kinetic energy and thus the same electron transmission function of the Specs Phoibos 150 NAP lens system (Ek ~ 300 eV). The number of photoelectrons detected per second from an orbital of constituent atoms can be quantified using the following equation (Handbook of X-ray Photoelectron Spectroscopy, Physical Electronics Division, Perkin-Elmer Corp., 1992),

$$I = nf\sigma\theta y\lambda AT,$$

where I is the number of photoelectrons detected per second from an orbital of constituent atoms; n is the number of atoms per cm^3 of the element of interest; f is the flux of X-ray photons impinging on the sample, in photons per $cm^{-2}s^{-1}$; σ is the photoelectric cross-section for the particular transition in cm^2 per atom; θ is the angular efficiency factor for the instrumental arrangement (angle between photon path and emitted photoelectron that is detected); y is the efficiency of production in the photoelectric process to give photoelectrons of normal energy (with final ionic state the ground state); λ is the mean free path of the photoelectrons in the sample. A is the area of the sample from which photoelectrons can be detected; T is the efficiency of detection of the photoelectrons emerging from the sample. In our experiments, these parameters (θ, y, λ, A, T) almost have the same values, and the peak intensity used in our calculation was already normalized by the photon flux [i.e., $(\boldsymbol{I_1/I_2}) = (I_1/I_2) \times (f_2)/(f_1)$]. Therefore, by comparing the ratio of peak area ($\boldsymbol{I}$) between the Xe 3d (cross section, $\sigma \sim 1.4672$) and Si 2p (cross section, $\sigma \sim 0.5421$), the ratio between the number of Si atoms and Xe atoms can be obtained through the equation, $n_{Si}/n_{Xe} = \boldsymbol{I}_{Si}/\boldsymbol{I}_{Xe} \times \sigma_{Xe}/\sigma_{Si}$. The total coverage of trapped Xe atoms was estimated at $\Theta = 0.08 \pm 0.02$ per nano-cage, which may be underestimated due to the existence of vitreous structures. Here, the coverage is defined as cages filled divided by the total number of cages. From the detailed peak intensities (Figure 1d), we know that the coverage of Xe_{int} is ~0.015 per nano-cage. (*Adapted from* J.Q. Zhong et al., *Nat. Commun.* **2017**, 8, 16118)

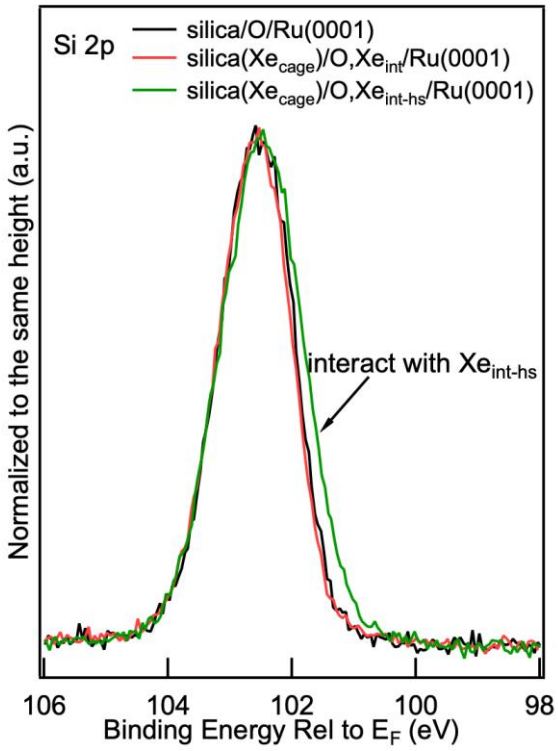

Figure S4. UHV XPS core level spectra of Si 2p. The black spectrum is obtained on clean silica bilayer (silica/O/Ru(0001)), the red spectrum is obtained after 1.4 torr Xe exposure for 10 minutes (silica(Xe_{cage})/O,Xe_{int}/Ru(0001)), and the green spectrum is obtained after 1.2 torr H_2 exposure for 10 minutes (silica(Xe_{cage})/O,Xe_{hs}/Ru(0001)). The green spectrum is shifted by 0.7 eV to the lower binding energy for clear comparisons. (Photon energy, $h\nu = 983$ eV)

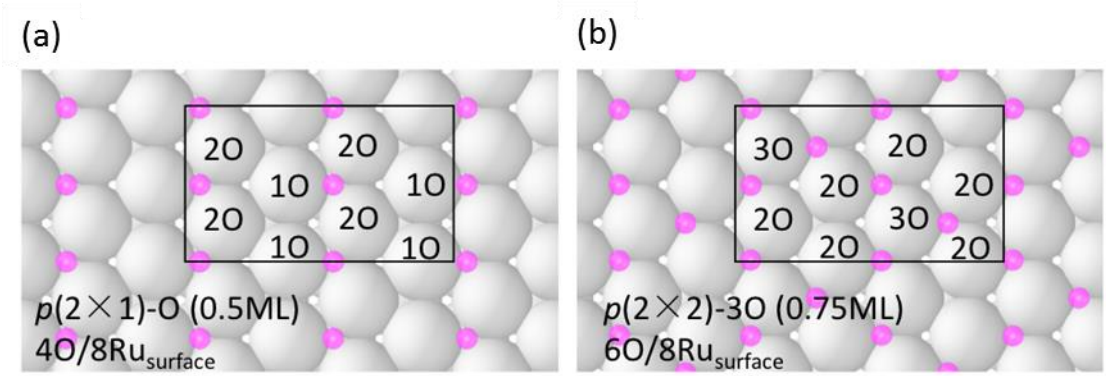

Figure S5. Interfacial chemisorbed oxygen (O_{int}) on Ru(0001). (a) *p*(2x1)-O phase (0.5ML) on Ru(0001) [50% surface Ru bonded with 1 O atom and 50% surface Ru bonded with 2 O atoms]. (b) *p*(2x2)-3O phase (0.75ML) on Ru(0001) [75% surface Ru bonded with 2 O atom and 25% surface Ru bonded with 3 O atoms].

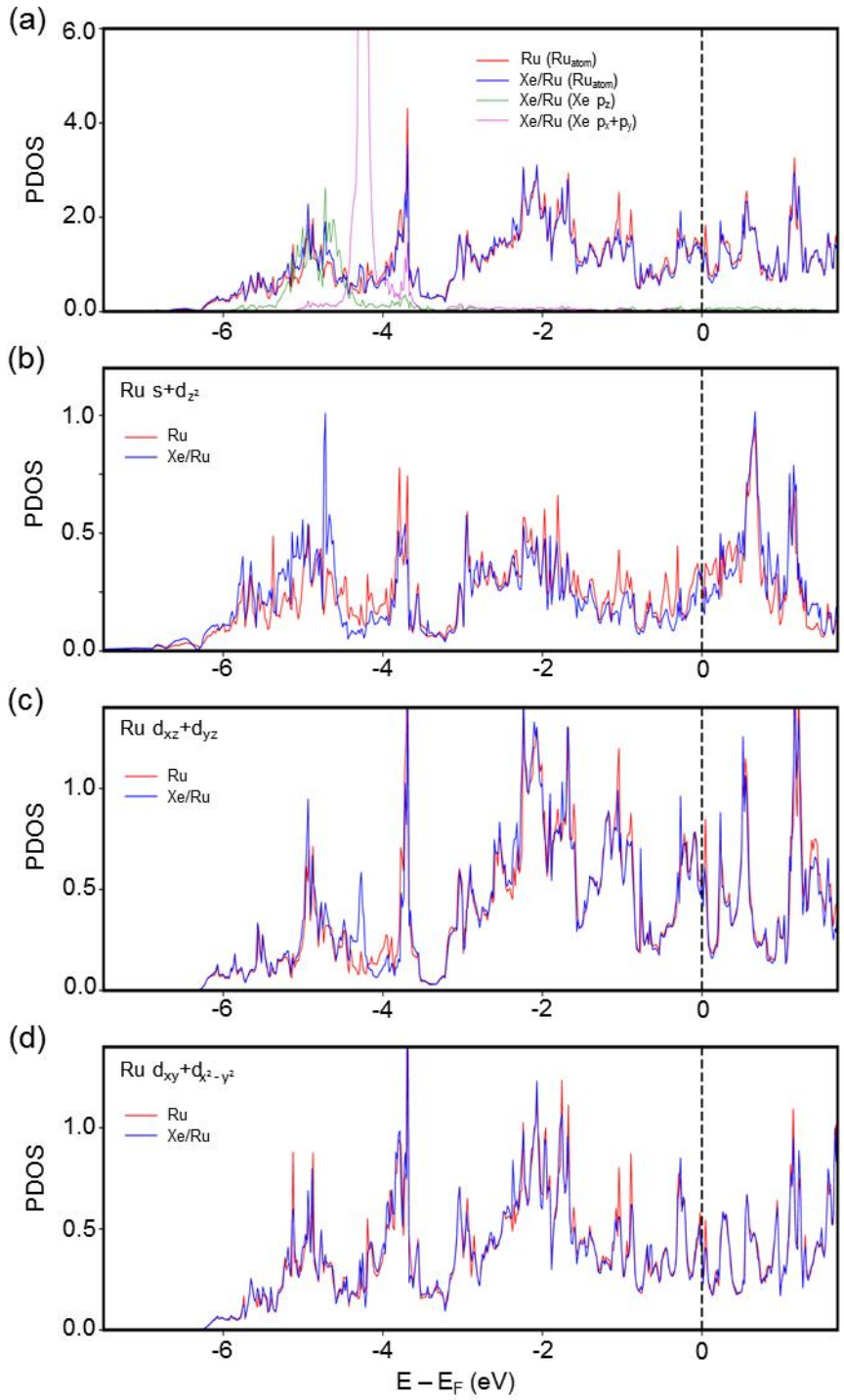

Figure S6. Projected density of states of Ru(0001) and Xe/Ru(0001). (a) PDOS of Ru *d* orbitals, Xe p_z orbital and Xe p_x+p_y orbitals. (b) PDOS of Ru s and d_{z^2} orbitals. (c) PDOS of Ru $d_{xz} + d_{yz}$ orbitals. (d) PDOS of Ru $d_{xy} + d_{x^2-y^2}$ orbitals. The energies are relative to E_F.

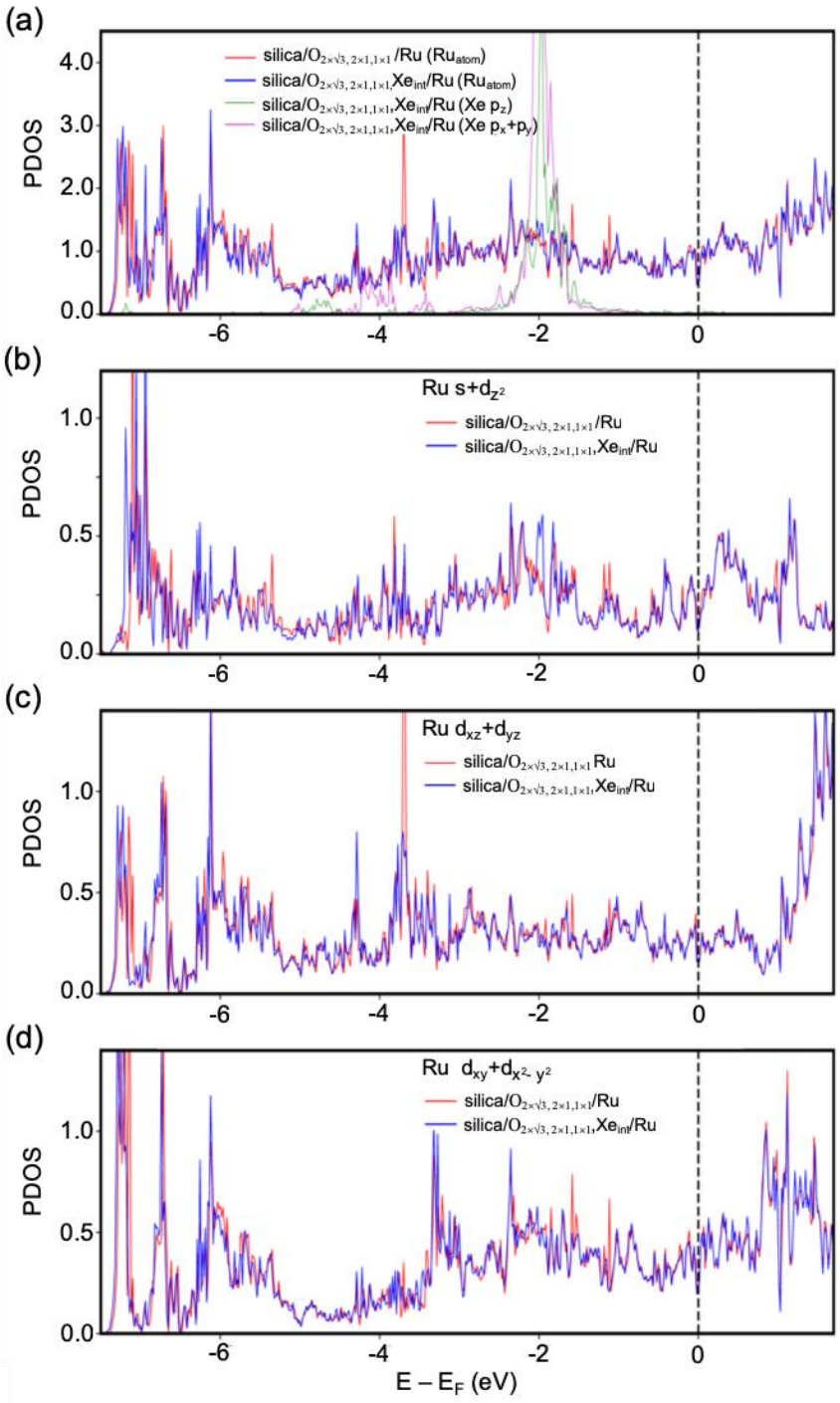

Figure S7. Projected density of states of silica/$O_{2\times\sqrt{3},\ 2\times1,1\times1}$/Ru(0001) and silica/$O_{2\times\sqrt{3},2\times1,1\times1,}Xe_{int}$/Ru(0001) with Xe_{int} adsorbed at *p*(1x1)-O domain. (a) PDOS of Ru *d*-orbitals, Xe p_z orbital and Xe p_x+p_y orbitals. (b) PDOS of Ru s and d_{z^2} orbitals. (c) PDOS of Ru $d_{xz} + d_{yz}$ orbitals. (d) PDOS of Ru $d_{xy} + d_{x^2-y^2}$ orbitals. The energies are relative to E_F.

Table S1. Normalized XPS peak areas (in %) for O 1s (Figure 1f).

	O 1s in silica	O 1s at the interface
Silica/O/Ru(0001) (black)	82	18
Silica(Xe_{cage})/O,Xe_{int}/Ru(0001) (red)	83	17

The coverage of interfacial chemisorbed oxygen (O_{int}) is determined by comparing the O 1s peak area between the silica (I_{O_silica}) and interface (I_{O_int}) as shown in Figure 1f. It should be noted that the interfacial chemisorbed oxygen is located underneath the silica bilayer framework (t ~ 0.426 nm). Therefore, we need to consider the attenuation effect for these O_{int} signal.

$$\boldsymbol{I_{O\_int}} = \boldsymbol{I_0} \cdot exp(-t_0/\lambda)$$

where $\boldsymbol{I_{O\_int}}$ is the measured XPS intensity for O_{int}, $\boldsymbol{I_0}$ is the real intensity for O_{int} without the attenuation effect, t_0 is the effective thickness of the silica bilayer (t_0 is assumed to be ~ 0.75t due to the porous nature of the bilayer framework), and λ (~ 1.15 nm) is the electron mean free path. For pristine silica/O/Ru(0001), the ratio of measured O 1s peak area is directly determined from the XPS spectra, i.e., $\boldsymbol{I_{O\_silica}}/\boldsymbol{I_{O\_int}}$ = 82/18. By considering the attenuation effect, then $\boldsymbol{I_{O\_silica}}/\boldsymbol{I_{O\_int}}$ = 82/24. For monolayer (1 ML) coverage of interfacial chemisorbed oxygen, there are 16 oxygen atoms in the silica and 8 oxygen atoms at the interface per unit cell. Therefore, based on ratio of $\boldsymbol{I_{O\_int}}/\boldsymbol{I_{O\_silica}}$ (0.29), we can estimate that there is 0.58 ML interfacial chemisorbed oxygen.